

PAPER • OPEN ACCESS

## Three-dimensional study of nodule clustering and heterogeneous strain localization for tailored material properties in ductile iron

To cite this article: Jakob Olofsson *et al* 2019 *IOP Conf. Ser.: Mater. Sci. Eng.* **529** 012078

View the [article online](#) for updates and enhancements.

# Three-dimensional study of nodule clustering and heterogeneous strain localization for tailored material properties in ductile iron

Jakob Olofsson<sup>1,\*</sup>, Kent Salomonsson<sup>1</sup>, Arne K. Dahle<sup>1</sup> and Ragnvald H. Mathiesen<sup>2</sup>

<sup>1</sup> Department of Materials and Manufacturing, School of Engineering, Jönköping University, Box 1026, SE-551 11 Jönköping, Sweden

<sup>2</sup> Department of Physics, Faculty of Natural Sciences, Norwegian University of Science and Technology, NTNU, NO-7491 Trondheim, Norway

\* Corresponding author: jakob.olofsson@ju.se

**Abstract.** Tailored heterogeneous distributions of microstructural features enable extraordinary material performance in biological and physiological structures such as trees, the aortic arch, human teeth and dinosaur skulls. In ductile iron, a heterogeneous distribution in size and morphology of graphite nodules and variations of the fractions of ferrite and pearlite are created during solidification, and varies as a function of parameters such as local cooling rate, segregation and flow. In the current work, the size distribution as well as the orientation and relation between graphite nodules is obtained by a three-dimensional reconstruction of a ductile iron microstructure from X-ray tomography. The effect of the nodule morphology and clustering on the localization of plastic strains is studied numerically using finite element analysis of the reconstructed microstructure. Real castings have a variation in geometry, solidification conditions and are subjected to variations in loads. A framework for optimized geometry and solidification conditions in order to design and deliver castings with tailored local material performance is proposed.

## 1. Introduction

Nature is filled with examples of structures where heterogeneous distributions of sub-scale features have been tailored to enable extraordinary performance when the structure is subjected to load. In trees, local microstructure variations are visibly seen as annual rings, but are also present as large-scale variations throughout the tree. This enable large deformations and absorption of energy when the tree is subjected to strong winds, and also makes the tree insensitive to damage initiation and crack propagation [1]. In the skulls of dinosaurs as well as humans, tailored local variations in the structure of bone enable efficient energy absorption when chewing, and makes the skull highly tolerant to damage [2,3].

Heterogeneous distributions of sub-scale features are also found in synthetic structures made in materials as concrete [4], injection moulded thermoplastics [5], and, not least, metal castings. Most metallic alloys solidify in a non-isothermal transformation through the nucleation and growth of phases, where factors such as chemical composition and local cooling rate affects the final morphology, refinement and amount of different phases. In shape casting, this inevitably leads to heterogeneous microstructures.



In ductile iron castings, the formation and growth of graphite nodules is highly related to the local solidification conditions, leading to spatial variations in nodule characteristics (size, morphology nodule count etc.) as well as in the iron matrix (e.g. volume fractions and refinements of ferrite and pearlite) [6]. In recent research, the formation and growth of graphite nodules have received much attention. Ghassemali *et al.* [7] used Focused Ion Beam (FIB) in a Scanning Electron Microscopy (SEM) to create serial sectioning images to reveal new insights behind the formation mechanism and growth of nodules. Azeem *et al.* [8] used synchrotron X-rays to investigate the graphite nucleation and growth in-situ during solidification. The size and morphology of the graphite nodules has been shown to be strongly related to the initiation and propagation of cracks when the material is subjected to load. Kasvayee *et al.* [9] used Digital Image Correlation (DIC) and in-situ tensile testing with optical microscopy to show that there is a strain localization between nodules, and that clustered nodules interact to form bands of high strain between them. As also pointed out by the authors, the study was performed as a 2D analysis, while the nodules actually interact in 3D. The results are in line with other studies showing that the crack propagation path is highly affected by the graphite nodules [10], and that the fracture process of ductile iron cannot be explained by theoretical models that consider the material as homogeneous [11].

In the current work, 3D reconstruction based on X-ray micro-tomography has been used to investigate the size distribution and clustering of nodules in ductile iron. Numerical simulations have been performed to demonstrate the strain localization and interaction between graphite nodules. If the effects of these variations can be better understood and controlled, there is a large potential to optimise these effects to enable tailored material performance also in shape castings. This paper aims to highlight current and future research in the area and demonstrate how increased knowledge about the formation and effect of graphite nodules can be utilized in an integrated simulation methodology to enable the use of tailored heterogeneous material behaviour in the design process for ductile iron castings.

## 2. Methods

The preparation of the material, the 3D reconstruction procedure as well as the creation of FE models is further described in accompanying work [12]. In brief, cylindrical samples with a diameter of 1 mm were machined from an industrial casting containing a pearlitic-ferritic matrix. X-ray tomography was performed using a Nikon XT H 225 CT scanner, with the samples positioned so that a voxel size of about 1  $\mu\text{m}$  was obtained. A reconstructed volume was generated where the nodules, ferrite and pearlite were segmented into separate volumes. From the reconstructed sample volume, a sub-volume was selected as a Representative Volume Element (RVE) in the shape of a cubic volume with a physical side length of about 0.7 mm. This RVE forms the basis for a Finite Element (FE) model, consisting of about 5 million linear tetrahedral elements. Material data for the different phases are assigned, assuming each phase to be homogeneous and isotropic. The boundary conditions for the load simulation of the micro-scale RVE is taken from a macro-scale load simulation of the ductile iron casting, a heavy truck engine support, performed using the so-called *closed chain of simulations for cast components* [6]. The load is applied in the form of a prescribed displacement vector of  $\mathbf{u} \approx (5.2, -3.5, 6.9)$   $\mu\text{m}$  on the top surface of the RVE, while the bottom surface is fixed. See [12] for additional details.

## 3. Results and Discussion

### 3.1. Nodule characteristics

The tomography data provides a lot of information about the morphology and 3D distribution of the nodules. In total, the volume is found to contain 135 nodules, corresponding to a volume fraction of 26.9%. An analysis of the sizes of the nodules, here measured by the nodules surface area, was first performed. Figure 1 shows the frequency plot for the nodule sizes, grouped into ranges of 0.002  $\text{mm}^2$  width. A representation of the nodule distribution is also shown in the figure, where the nodules are represented by idealised spheres of the same surface area as the real nodules. Most of the nodules are found to have a surface area in the range 0.002-0.004  $\text{mm}^2$ ; 43 of the 135 nodules, or 32%, are found in this range. There is also a slight peak of nodules with a surface area of about 0.015  $\text{mm}^2$ , where 13

nodules are found (9.6%). Only 7 nodules have a surface area larger than this, thus in total about 15% of the nodules are found in the range with a surface area of 0.015 mm<sup>2</sup> or larger.

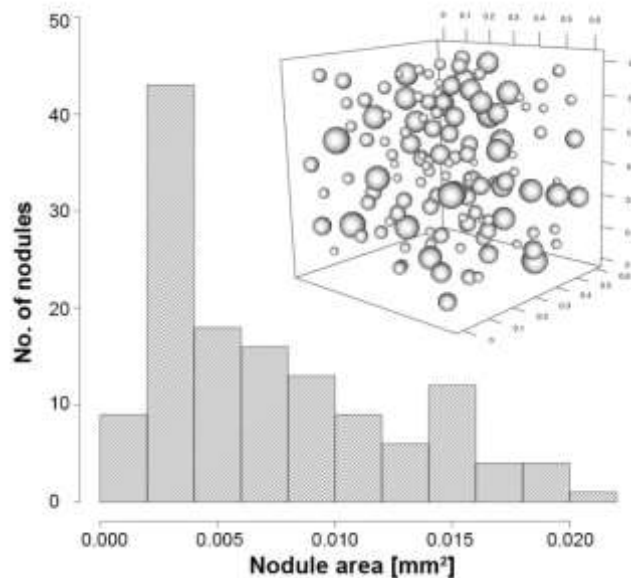


**Figure 1.** Frequency plot of the nodule sizes found in the RVE. The inserted graphic shows the distribution of the idealised spherical nodule representations in the volume.

Looking at the volumetric nodule size distribution, the frequency plot looks very different. Figure 2a shows the nodule volume fraction for the groups with different nodular diameters. The figure shows that there is one group that stands out; the group with a diameter of about 35  $\mu\text{m}$  contains 22% of the graphite volume. The largest group of nodules in terms of numbers, with an average diameter of 15  $\mu\text{m}$ , only contain about 7% of the total graphite volume.

The results highlight the difficulty in describing the 3D characteristics and size distribution of the nodules. The average nodule diameter in this dataset is 23  $\mu\text{m}$ , but that is a value which only describes about 12% of the number of nodules. The largest group in number (diameter around 15  $\mu\text{m}$ ) only describes 7% of the graphite volume, and the largest graphite volume is found in only 9% of the nodules.

By plotting the cumulative fractions of both the number of nodules and their volumes, Figure 2b is obtained. It can be seen that though 80% of the number of nodules are found in the groups with an average diameter up to 30  $\mu\text{m}$ , these nodules only contain 45% of the graphite volume. Nodules larger than or equal to 35  $\mu\text{m}$  are found to contain the same volume fraction graphite (45%), though only being 15% of the number of nodules. The cumulative distribution also shows that there is a clear step in volume fractions at a nodule diameter of 35  $\mu\text{m}$ . Comparing the cumulative distributions of the number of nodules and the nodular volume fraction in the same figure, Figure 3a is obtained. It can be seen that both curves have a clear step at a nodule diameter of 35  $\mu\text{m}$ . In Figure 3b, the data is visualised as a bubble diagram, where the size of each bubble represents the number of nodules in each group.

These figures indicate that the nodules can be seen as two different populations; one with diameters larger than 35  $\mu\text{m}$ , and one with smaller diameter, which is interesting from a solidification and nodule growth perspective. There is clearly a small group of large nodules (larger than or equal to 35  $\mu\text{m}$ ) that contain 45% of the graphite volume. It is suggested that this population may have nucleated before the second population with smaller nodules. It is possible that the use of nucleation agents and local cooling conditions have led to preferential nucleation sites in the melt where nodules have nucleated freely, maybe already before the nucleation of austenite. These nodules would then grow without the influence of surrounding austenite, which would be the case if the nodules formed between dendrite arms. This was not observed in the before-mentioned synchrotron study at a very low cooling rate [8], but is likely

to occur at higher cooling rates, depending also on the use and effect of nucleation agents. It is not in the scope of the current work to further elaborate on the mechanisms behind this, but we here highlight that there are still aspects of the nucleation and growth of nodules that needs to be addressed in future work. Additional studies of several different volumes are required, as well as further studies of the nucleation mechanisms, solidification paths and nodule growth behaviour.

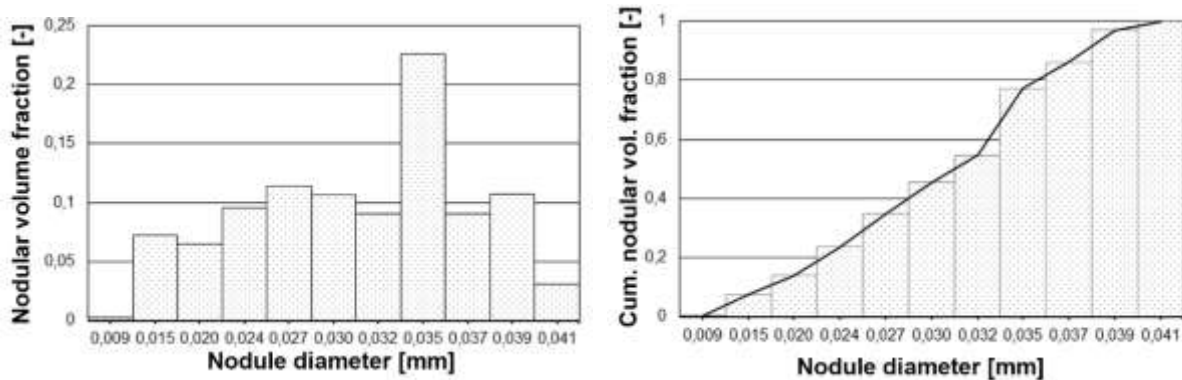


**Figure 2.** a) The nodular volume fraction for the different nodule sizes. c) The cumulative nodular volume fractions for the different nodule sizes.

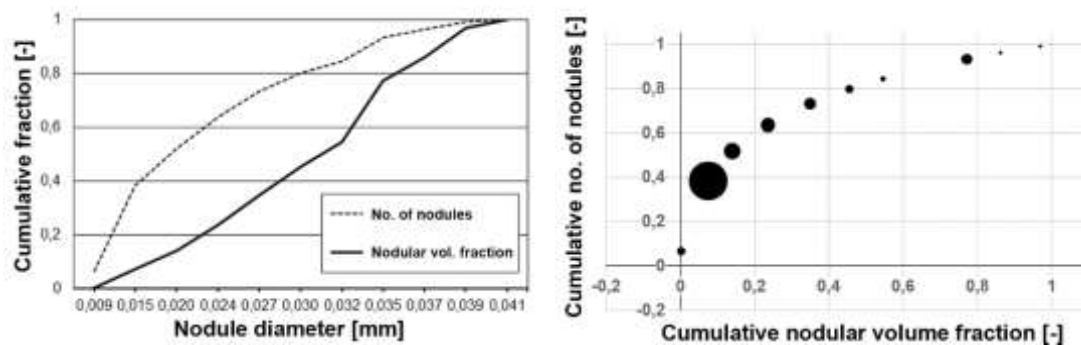


**Figure 3.** a) Comparison of cumulative fractions of the number of nodules and the nodular volume fraction. b) Bubble diagram of the cumulative fractions, where the size of the bubble represents the number of nodules in the different groups.

Since there is a clear nodule size variation, it is also important to know if nodules of different sizes are evenly distributed or if they are clustered. In the current study, the large nodules, with a diameter of 35  $\mu\text{m}$  or more, are selected for further investigation of the three-dimensional arrangement of the nodules. By investigating how closely they are positioned to each other, a dendrogram can be constructed. The obtained dendrogram is shown in Figure 4a, and the location of the large nodules in the volume is shown in Figure 4b. The dendrogram shows that these large nodules are indeed not evenly distributed in the volume, but instead positioned in three distinct main clusters, with a distance of about 100  $\mu\text{m}$  between the nodules in the clusters. There can be different reasons for this clustering, and indeed the investigated volume is not sufficient to draw any real conclusions. However, we suggest that if these nodules are indeed nucleated freely in the melt, they may have been pushed to these areas by the growing austenite, and/or affected by other forces as convection or gravity. Additional studies are required to understand and control the nucleation and growth mechanisms properly.

The results also highlight the limited capacity of 2D sectioning to characterise the nodule characteristics; randomly selected 2D sections through this 3D volume would yield very different views of the nodule characteristics depending on their position and would not necessarily reveal the clustering of large nodules or the complex size/volume distribution of graphite.

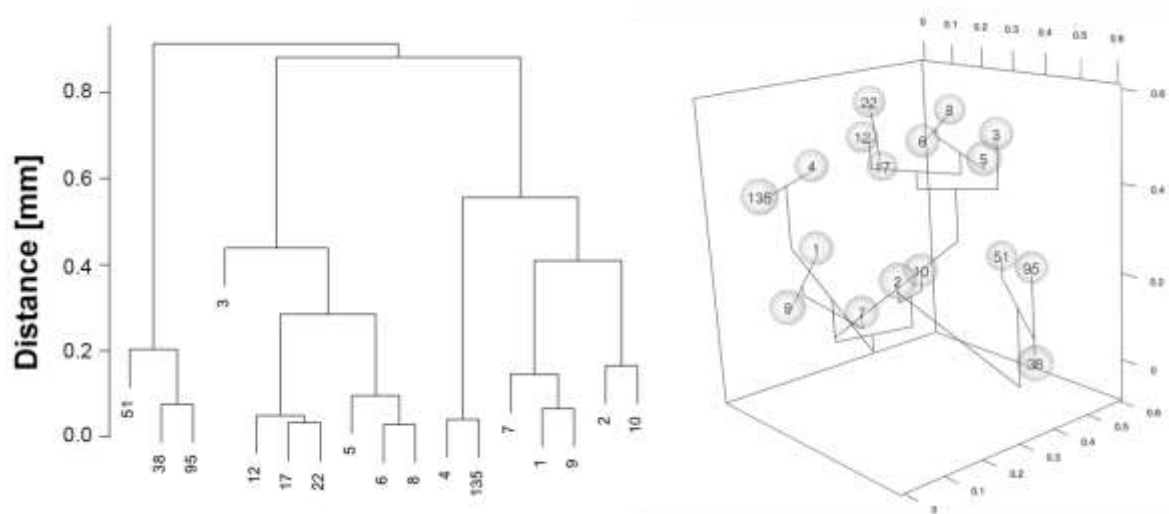


**Figure 4.** Dendrogram showing the clustering of nodules, as well as their distribution and connections throughout the volume. Only nodules with diameter 35  $\mu\text{m}$  and larger are considered.

### 3.2. FE results

Turning to the FE simulation results, it is observed that the nodules of different sizes interact to form bands of localised strains between them. The results are further described in [12]. In the current simulations, no initial stresses are prescribed in the microstructure. As recently shown by Andriollo *et al.* [13], local residual stresses are formed around the nodules during solidification due to the larger thermal contraction by the matrix compared to the nodules during solid-state cooling. This is expected to contribute to the strain localization, but here the effect and magnitude of this contribution has not been investigated or considered. In addition, the phases are here modelled as homogeneous, which particularly for graphite is a simplification that not completely resembles the real behaviour [14]. The present simulation is thus simplified, but useful to reveal the three-dimensional interaction between non-uniformly distributed nodules. Future work could focus on combining these aspects to investigate how the internal structure of the graphite and the residual stresses around the nodules act in combination with the non-uniform spatial distribution to affect the mechanical performance.

### 3.3. Simulation methodology

In previous work, a closed chain of simulations for cast components has been developed, where casting process simulation is applied to model the variations in microstructure and mechanical behaviour throughout a casting, which is incorporated into a load analysis of the casting in use [6]. This enables an integrated simulation approach which spans casting process, microstructure formation and solidification modelling as well as in-use behaviour of castings. By adopting a knowledge-based perspective, this approach serves as the basis for a framework for an integrated optimization loop [15]. Here the geometry as well as casting process parameters act as variables to tailor the heterogeneous material behaviour in the casting in a multi-objective optimization perspective. This enables the prediction and optimization of heterogeneous material behaviour in the design and development. However, to fully utilize the potential of tailored material properties in industrial castings, there are still research challenges related to understanding and optimizing the nucleation and growth of microstructural features, e.g. graphite nodules, as highlighted in the current work.

## 4. Conclusions

The three-dimensional characteristics of nodules in a ductile iron is investigated, where it is found that:

- Though there is a large population of small nodules, they only represent a small part of the volume fraction nodules.

- There is a small population of large nodules, 15% of the number of nodules, that contain about 45% of the total volume fraction nodules.
- The large nodules are found to be non-uniformly distributed, clustered into three main groups.

The findings are discussed and elaborated, and topics to be addressed in future research are suggested. An integrated simulation-based design approach to tailor and optimize the local variations in microstructure of industrial castings have been highlighted.

### Acknowledgement

The authors would like to acknowledge the Swedish Knowledge Foundation for financial support of the research project ODISSEE2 and the research profile CompCAST+, both part of the research environment SPARK at Jönköping University.

### References

- [1] Barnett J R and Bonham V A 2004 Cellulose microfibril angle in the cell wall of wood fibres *Biol. Rev. Camb. Philos. Soc.* **79** 461–72
- [2] Rayfield E J, Norman D B, Horner C C, Horner J R, Smith P M, Thomason J J and Upchurch P 2001 Cranial design and function in a large theropod dinosaur *Nature* **409** 1033–7
- [3] Wroe S, Moreno K, Clausen P, McHenry C and Curnoe D 2007 High-resolution three-dimensional computer simulation of hominid cranial mechanics *Anat. Rec.* **290** 1248–55
- [4] Bazant Z P 1976 Instability, ductility, and size effect in strain-softening concrete *ASCE J. Eng. Mech. Div.* **102** 331–44
- [5] Michaeli W and Baranowski T 2010 Simulation of the microstructure formation in injection molded semicrystalline thermoplastic parts *J. Polym. Eng.* **30** 29–41
- [6] Olofsson J and Svensson I L 2012 Incorporating predicted local mechanical behaviour of cast components into finite element simulations *Mater. Des.* **34** 494–500
- [7] Ghassemali E, Hernando J C, Stefanescu D M, Dioszegi A, Jarfors A E W, Dluhoš J and Petre nec M 2019 Revisiting the graphite nodule in ductile iron *Scr. Mater.* **161** 66–9
- [8] Azeem M A, Bjerre M K, Atwood R C, Tiedje N and Lee P D 2018 Synchrotron quantification of graphite nodule evolution during the solidification of cast iron *Acta Mater.* **155** 393–401
- [9] Kasvayee K A, Salomonsson K, Ghassemali E and Jarfors A E W 2016 Microstructural strain distribution in ductile iron; comparison between finite element simulation and digital image correlation measurements *Mater. Sci. Eng. A* **655** 27–35
- [10] Iacoviello F, Di Bartolomeo O, Di Cocco V and Piacente V 2008 Damaging micromechanisms in ferritic–pearlitic ductile cast irons *Mater. Sci. Eng. A* **478** 181–6
- [11] Berdin C, Dong M J and Prioul C 2001 Local approach of damage and fracture toughness for nodular cast iron *Eng. Fract. Mech.* **68** 1107–17
- [12] Salomonsson K and Olofsson J 2017 Analysis of localized plastic strain in heterogeneous cast iron microstructures using 3D finite element simulations *Proc. of the 4th World Congress on Integrated Computational Materials Engineering (ICME 2017, Ypsilanti)* ed P Mason *et al.* (Springer International Publishing) pp 217–25
- [13] Andriollo T, Hellström K, Sonne M R, Thorborg J, Tiedje N and Hattel J 2018 Uncovering the local inelastic interactions during manufacture of ductile cast iron: How the substructure of the graphite particles can induce residual stress concentrations in the matrix *J. Mech. Phys. Solids* **111** 333–57
- [14] Andriollo T, Thorborg J and Hattel J 2016 Modeling the elastic behavior of ductile cast iron including anisotropy in the graphite nodules *Int. J. Solids Struct.* **100–101** 523–35
- [15] Olofsson J, Salomonsson K, Johansson J and Amouzgar K 2017 A methodology for microstructure-based structural optimization of cast and injection moulded parts using knowledge-based design automation *Adv. Eng. Softw.* **109** 44–52